

Type Ia supernovae have two physical width-luminosity relations and they favor sub-Chandrasekhar and direct collision models

I. Bolometric

Nahliel Wygoda,^{1,2}★ Yonatan Elbaz² Boaz Katz¹

¹*Dept. of Particle Phys. & Astrophys., Weizmann Institute of Science, Rehovot 76100, Israel*

²*Dept. of Physics, NRCN, Beer-Sheva 84190, Israel*

Accepted XXX. Received YYY; in original form ZZZ

ABSTRACT

While the width-luminosity relation (WLR) among type Ia supernovae (slower is brighter) has been extensively studied, its physical basis has not been convincingly identified. In particular, the ‘width’ has not been quantitatively linked yet to a physical time scale. We demonstrate that there are two robust fundamental time scales that 1. can be calculated based on integral quantities of the ejecta, with little dependence on radiation transfer modeling and 2. can be inferred from observations. The first is the gamma-ray escape time t_0 , which determines the long-term evolution of the bolometric light curve and is studied in this Paper I. The second is the recombination time of ^{56}Fe and ^{56}Co , which sets the long-term color evolution of the emitted light and is studied in Paper II. Here we show that the gamma-ray escape time t_0 can be derived with $\sim 15\%$ accuracy from bolometric observations based on first principles. When applied to a sample of supernovae, the observed values of t_0 span a narrow range of 30 – 45 days for the wide range of observed ^{56}Ni masses $0.1M_{\odot} \lesssim M_{^{56}\text{Ni}} \lesssim 1M_{\odot}$. This narrow range of the gamma-ray escape time across the range of luminosities (a trivial WLR) is consistent with central detonations and direct collisions of sub-Chandrasekhar mass white dwarfs (WDs) but not with delayed detonation models for explosions of Chandrasekhar mass WDs, which are therefore disfavored as the primary channel for the population of type Ia supernovae. Computer codes for extracting t_0 from observations and models and for calculating gamma-ray transfer in 1D-3D are provided.

Key words: radiative transfer – Supernovae: Type Ia

1 INTRODUCTION

There is strong evidence suggesting that type Ia SNe, which comprise most of the observed SNe, are the result of thermonuclear explosions of WDs (see e.g. the recent reviews Hillebrandt & Niemeyer (2000); Maoz et al. (2014)). But what triggers the explosion in some (about 1% of) WDs to produce type Ia SNe remains an open question. Ideas that have been put forth can be separated based on the mass of the exploding WD, including 1. Chandrasekhar mass models (M_{ch} models): WDs close to the Chandrasekhar mass which are triggered by central heating due to continuing accretion (e.g. Hoyle & Fowler (1960); Arnett (1969); Khokhlov (1991)) 2. Sub-Chandrasekhar mass models (sub- M_{ch} models): massive WDs with mass of about $\approx 1M_{\odot}$ which are triggered by the explosion of a helium shell during accretion (e.g. Woosley et al. (1986); Livne (1990); Shen & Bildsten (2014); Shen et al. (2017)) or by a violent merger with another WD (e.g.

Pakmor et al. (2010)). 3. Collisions: direct collisions of typical WDs with masses $\approx 0.5 - 1M_{\odot}$ (e.g. Rosswog et al. (2009); Katz & Dong (2012); Kushnir et al. (2013); Dong et al. (2015)).

Most of the observed data on type Ia supernovae consists of spectra and light curves in the optical regime. It has long been realized that type Ia supernovae span a significant range in luminosities (peak luminosity varying in the range $10^{42} - 10^{43}$ ergs/s) which are correlated with the timescales for the rise and decline of the light in the different bands (e.g. Pskovskii (1977); Phillips (1993, 2005)). Quite generally, brighter type-Ia tend to evolve more slowly. This so called width-luminosity relation (WLR) is crucial for using type Ia’s as standard candles.

The brightness of a type Ia is mostly set by the amount of ^{56}Ni produced. The observed range of brightness implies that the progenitors have a spread in ^{56}Ni yield in the range $0.1M_{\odot} \lesssim M_{^{56}\text{Ni}} \lesssim 1M_{\odot}$. But which feature of the explosion sets the evolution time-scale and what does the correlation teach us about the ejecta? It has become clear that both the temporal evolution of the bolometric light curve (e.g. Pinto & Eastman

★ E-mail: nahliel.wygoda@weizmann.ac.il

(2000, 2001)) and the color (e.g. Kasen & Woosley (2007)) are important and may depend on the properties of the ejecta. A particularly important question for making progress with identifying the explosion mechanism is the relation to the total ejected mass. Is the sequence hinting to a spread of masses (e.g. Phillips (1993); Pinto & Eastman (2000); Kushnir et al. (2013); Scalzo et al. (2014a); Blondin et al. (2017)) or is it a result of composition variations in explosions that all eject M_{ch} (e.g. Hoefflich et al. (1996); Pinto & Eastman (2001); Mazzali et al. (2001); Kasen & Woosley (2007); Hoefflich et al. (2017))? The results presented here provide evidence that the range of type Ia's is not likely to originate from M_{ch} explosions.

It is important to note that while some studies investigate the entire range of observed brightness (e.g. Sim et al. (2010); Blondin et al. (2017); Hoefflich et al. (2017)), other studies ignore the faint end and focus only on the bright part of the relation (e.g. Pinto & Eastman (2001); Mazzali et al. (2001); Kasen & Woosley (2007)), assuming that there is a separate mechanism causing the low end. Yet other studies (Dhawan et al. 2017) have shown that the observation of separate subclasses at the low luminosity end might point to the presence of several explosion mechanisms. Given the continuous distribution of type Ia photometric (e.g. Phillips (2005)) and spectroscopic properties (e.g. Nugent et al. (1995); Branch et al. (2009)), and the success of some calculations in producing the full range of brightness (e.g. Hoefflich et al. (1996); Sim et al. (2010); Kushnir et al. (2013)) it is possible that the majority of type Ia's across the brightness range originate from a single underlying mechanism with continuous parameters. In this paper we study the WLR across the entire brightness range.

Studies of the emission from type Ia face the following significant challenges: First, we don't know the explosion scenario, allowing a very large parameter space of possibilities to study. Second, given a specific scenario, the calculation of the explosion and radiation transfer requires the use of approximations which are not clearly valid to sufficient accuracy. A nice demonstration of the challenge in radiation transfer modeling is the recent 1-D calculations of two of the most popular models by three different groups this year (Shen et al. 2017; Blondin et al. 2017; Hoefflich et al. 2017), which obtain contradictory results of the WLR for essentially the same explosion scenarios: compare the core detonation sub-Chandra models in figure 13 of Shen et al. (2017) to those in figure 5 of Blondin et al. (2017) and the delayed detonation Chandra models in figure 5 of Blondin et al. (2017) to those in figure 8 of Hoefflich et al. (2017).

In order to make progress, we believe it is essential to identify **robust and quantitative** features of models and observations which are insensitive to the uncertainties of radiation transfer.

Energy conservation can be used to bypass detailed radiation transfer if the bolometric light curve can be accurately inferred from observations. One robust parameter which can be inferred from the bolometric light curve is the mass of ^{56}Ni , which largely sets the brightness scale of the light curve. Another parameter which would be very useful to infer is the total mass of the ejecta M_{tot} (e.g. Scalzo et al. 2014a). While there is no known way to infer the total mass in a model-independent way, the total column density (weighted by ^{56}Ni) can be inferred from the shape of the light curve at late times (e.g. Jeffery 1999). The total column density sets the average optical depth for gamma-rays at late times and is parametrized by the gamma-ray escape time t_0 (defined such that at late times, $t \gg t_0$, the fraction of energy in gamma-rays that is deposited in the ejecta is t_0^2/t^2 , see §2). t_0 is a fundamental time scale in the evolution of the light curve and in particular sets the slope of the decline of the bolometric light.

In this Paper I we present a new method to derive the total ^{56}Ni mass and the gamma-ray escape time t_0 which is simple and directly based on energy conservation. We show that these parameters are robust, and quantify the estimated uncertainty in their inference. We apply this method to bolometric light curves from the literature to study the physical relationship between t_0 and ^{56}Ni , which we call the "bolometric WLR" (and is different from the "usual" WLR which refers to various bands of the spectrum). In Wygoda et al. (2018) (hereafter Paper II) we study a second physical time-scale which is fundamental to the WLR, namely the time of recombination of iron group elements from doubly ionized to singly ionized. We show that it can be robustly calculated theoretically and inferred from observations using the distinctive brake in the color evolution of type Ia's around 30 days after peak (Burns et al. 2014; Pskovskii 1977, e.g.). Any successful model needs to agree with the two WLRs obtained from the bolometric and the color time scales. By comparing the results of representative models of Chandrasekhar, sub-Chandrasekhar and direct collision scenarios, we find that all agree with the color WLR but only the sub-Chandrasekhar and direct collisions are consistent with the bolometric WLR. Chandrasekhar-mass models are consistent with bright type Ias and are inconsistent with faint type Ia's.

This Paper I is organized as follows. In §2, a method to infer ^{56}Ni mass and t_0 from observed light-curves is derived based on energy conservation arguments. In §3, detailed 1-D radiation transfer calculations are used to validate the method for representative models and study the sensitivity to the quality of the observed light-curve and level of approximation. In §4, the method is applied to extract the parameters from samples of tens of observed SNIa. In §5, the observed ejecta parameters are compared to Chandrasekhar, sub-Chandrasekhar and direct collision scenarios. The results are summarized in §6. The analysis files in python (Jupyter notebooks) and matlab, as well as a c-based gamma-ray Monte Carlo code are provided with the manuscript and are described in appendix §A.

2 THE GAMMA-RAY ESCAPE TIME AND ^{56}Ni MASS CAN BE DIRECTLY EXTRACTED FROM BOLOMETRIC LIGHT CURVES

In this section we describe how the ^{56}Ni mass and gamma-ray escape time t_0 can be extracted from bolometric UVOIR light curves.

2.1 Energy conservation connects the deposition rate to the bolometric light curve

The radioactive decay chain of ^{56}Ni emits energy in the form of γ -rays and positrons which traverse the ejecta. At any given time t , the gamma-rays and positrons deposit some of their energy in the ejecta plasma at a total rate of Q_{dep} which is essentially instantaneously converted to UVOIR radiation. The total energy deposition rate $Q_{dep}(t)$ can be accurately calculated using a gamma-ray transport code or approximated analytically (see §2.2). It is important to emphasize that the physics of gamma-ray transfer is well understood. The dominant interaction of gamma-rays with the plasma is Compton collisions with all electrons and is practically independent of temperature and ionization. Each gamma-ray photon can be calculated separately using Monte-Carlo simulations. The total deposition rate for any 3D model ejecta can be calculated easily and accurately (a Monte Carlo code is attached to the manuscript and described in appendix §A). The question we address here is how to

relate the total deposition rate Q_{dep} to the UVOIR bolometric light curve L_{bol} .

At sufficiently late times after explosion, the diffusion time becomes much shorter than the dynamical time and energy deposited is immediately emitted:

$$L_{\text{bol}}(t) = Q_{\text{dep}}(t) \text{ for } t \gg t_{\text{peak}}. \quad (1)$$

At early times the UVOIR radiation is trapped and the deposition cannot be directly related to the emission. As the radiation diffuses through the ejecta its energy is diluted adiabatically due to the expansion and the integrated emission is smaller than the integrated deposition $\int dt L_{\text{bol}}(t) < \int dt Q_{\text{dep}}(t)$. Since the expansion is adiabatic to an excellent approximation, the time weighted energy in the radiation is conserved and we have $tE_{\text{rad}}(t) + \int dt t L_{\text{bol}}(t) = \int dt t Q_{\text{dep}}(t)$, where $E_{\text{rad}}(t)$ is the total energy in UVOIR radiation in the ejecta at time t (Katz et al. 2013). At late times there is little trapped radiation and to a good approximation we have

$$\int_0^t dt' t' L_{\text{bol}}(t') = \int_0^t dt' t' Q_{\text{dep}}(t') \text{ for } t \gg t_{\text{peak}}. \quad (2)$$

Thus, given an ejecta model and the corresponding Q_{dep} , the model can be compared to actual observations using Eqs. (1) and (2). In particular, it is useful to compare the ratios of the two equations (Kushnir et al. 2013, see also figure 1):

$$\frac{L_{\text{bol}}(t)}{\int_0^t dt' t' L_{\text{bol}}(t')} = \frac{Q_{\text{dep}}(t)}{\int_0^t dt' t' Q_{\text{dep}}(t')} \text{ for } t \gg t_{\text{peak}}. \quad (3)$$

The ratios in equation (3) do not depend on the distance or the total amount of ^{56}Ni (both numerator and denominator scale linearly with the ^{56}Ni fraction) and thus provide direct information on the gamma-ray escape fraction (Kushnir et al. 2013).

2.2 The deposition rate is set by the ^{56}Ni mass and the gamma-ray escape time t_0

The rate of energy deposition in the ejecta from γ -rays can be precisely expressed analytically in two limits: 1. At early times, when the ejecta is dense enough that all γ -rays are trapped and their energy is fully deposited in the ejecta, the gamma-ray deposition fraction $f_{\text{dep},\gamma}$ is:

$$f_{\text{dep},\gamma} = 1 \text{ at } t \lesssim t_{\text{peak}}. \quad (4)$$

2. At late times the ejecta becomes optically thin to gamma-rays and each gamma-ray has a small chance to experience a Compton collision (and negligible chance to have more than one collision). The deposition is thus accurately accounted for by an effective opacity κ_{eff} which is calculated by averaging the Klein-Nishina corrected Compton cross section $\Sigma_C(E_n)$ and average fractional energy loss per scattering $\langle dE \rangle / E$ over each of the (discrete) emitted gamma-ray energies E_n (including the positron annihilation line Swartz et al. 1995; Jeffery 1999)

$$\kappa_{\text{eff}} = Y_e \sum_{\gamma \text{ lines}} f_n \frac{\sigma_C(E_n)}{m_p} \frac{\langle dE \rangle_n}{E_n} \approx 0.025 \text{ cm}^2/\text{gr} \quad (5)$$

where f_n is the fraction of energy emitted in the line n , and it was assumed that there are two baryons per electron ($Y_e = 0.5$). The gamma-ray deposition fraction at late times is given by

$$f_{\text{dep},\gamma} = \kappa_{\text{eff}} \langle \Sigma \rangle_{\text{Ni}} = \frac{t_0^2}{2} \text{ at } t \gg t_{\text{peak}}, \quad (6)$$

where $\langle \Sigma \rangle_{\text{Ni}} \propto t^{-2}$ is the average column density of the ejecta as seen by the ^{56}Ni elements:

$$\langle \Sigma \rangle_{\text{Ni}} = \int \frac{d^3x}{M_{\text{Ni}56}} \rho_{\text{Ni}56}(\mathbf{x}) \int \frac{d\hat{\Omega}}{4\pi} \int_0^\infty ds \rho(\mathbf{x} + s\hat{\Omega}) \quad (7)$$

where $\rho_{\text{Ni}56}$ is the density of ^{56}Ni and ρ is the total density. The escape time t_0 is given by

$$t_0 = \sqrt{\kappa_{\text{eff}} t^2 \langle \Sigma \rangle_{\text{Ni}56}} \quad (8)$$

and is independent of time (assuming homologous expansion). At times $t \gtrsim t_0$ a significant fraction of the emitted gamma-rays escape the ejecta without depositing their energy. t_0 can be easily calculated for any ejecta using equation (8). A Python based code to calculate t_0 for 1-D ejecta and c-based codes for calculating the gamma-ray transport and t_0 for 1-D, 2-D and 3-D are provided in the attached material as described in appendix §A.

A useful interpolation for the deposition function between the two exact limiting values in Eqs. (4) and (6) is (e.g. Scalzo et al. 2014a)

$$f_{\text{dep},\gamma}(t) \approx 1 - e^{-\left(\frac{t_0}{t}\right)^2}. \quad (9)$$

The total deposition rate at any time can be thus approximated by:

$$Q_{\text{dep}}(t) \approx Q_\gamma(t) \cdot \left(1 - e^{-\left(\frac{t_0}{t}\right)^2}\right) + Q_{\text{pos}}(t) \quad (10)$$

where Q_γ and Q_{pos} are the total energy release rate of gamma-rays and positron kinetic energy respectively and are given by:

$$\begin{aligned} Q_\gamma(t) &= N_{\text{Ni}} \cdot \left[\frac{Q_{\text{Ni}}}{\tau_{\text{Ni}}} \cdot e^{-\frac{t}{\tau_{\text{Ni}}}} + \frac{Q_{\text{Co},\gamma}}{\tau_{\text{Co}} - \tau_{\text{Ni}}} \cdot \left(e^{-\frac{t}{\tau_{\text{Co}}}} - e^{-\frac{t}{\tau_{\text{Ni}}}} \right) \right] \\ &= \frac{M_{\text{Ni}56}}{M_\odot} \left[6.45 e^{-\frac{t}{8.76\text{d}}} + 1.38 e^{-\frac{t}{111.4\text{d}}} \right] \times 10^{43} \text{ ergs/s} \end{aligned} \quad (11)$$

and

$$\begin{aligned} Q_{\text{pos}}(t) &= N_{\text{Ni}} \cdot \frac{Q_{\text{Co, pos}}}{\tau_{\text{Co}} - \tau_{\text{Ni}}} \cdot \left(e^{-\frac{t}{\tau_{\text{Co}}}} - e^{-\frac{t}{\tau_{\text{Ni}}}} \right) \\ &= 4.64 \frac{M_{\text{Ni}56}}{M_\odot} \left[-e^{-\frac{t}{8.76\text{d}}} + e^{-\frac{t}{111.4\text{d}}} \right] \times 10^{41} \text{ ergs/s} \end{aligned} \quad (12)$$

where N_{Ni} is the number of synthesized ^{56}Ni nuclei, the lifetimes of ^{56}Ni and ^{56}Co are $\tau_{\text{Ni}} = 8.76$ days and $\tau_{\text{Co}} = 111.4$ days, respectively (Junde 1999), the mean γ -ray energies per decay are $Q_{\text{Ni}} = 1.73$ Mev, $Q_{\text{Co},\gamma} = 3.57$ Mev (Ambwani & Sutherland 1988) and $Q_{\text{Co, pos}} = 0.12$ Mev. Note that at very late times of hundreds of days past explosion positrons may escape the ejecta [see e.g. constraints by Axelrod (1980) and Kerzendorf et al. (2014)].

2.3 Extracting t_0 and ^{56}Ni from light curves

The luminosity ratio $L_{\text{bol}}(t) / \int_0^t L_{\text{bol}}(t') dt'$ can be used to extract t_0 using Eqs. (3) and (10-12). In the top right panel of figure 1 the luminosity ratios of five well observed supernovae from the literature that include UV, optical and IR observations are shown. For convenience the luminosity ratios are multiplied by $t^{2.5}$, where t is the estimated time since explosion in days. The expected ratios for a range of t_0 values, as given by Eqs. (3) and (10-12), are shown in black lines with labels indicating the corresponding values of t_0 . As can be seen in the figure, the light-curves of all five supernovae

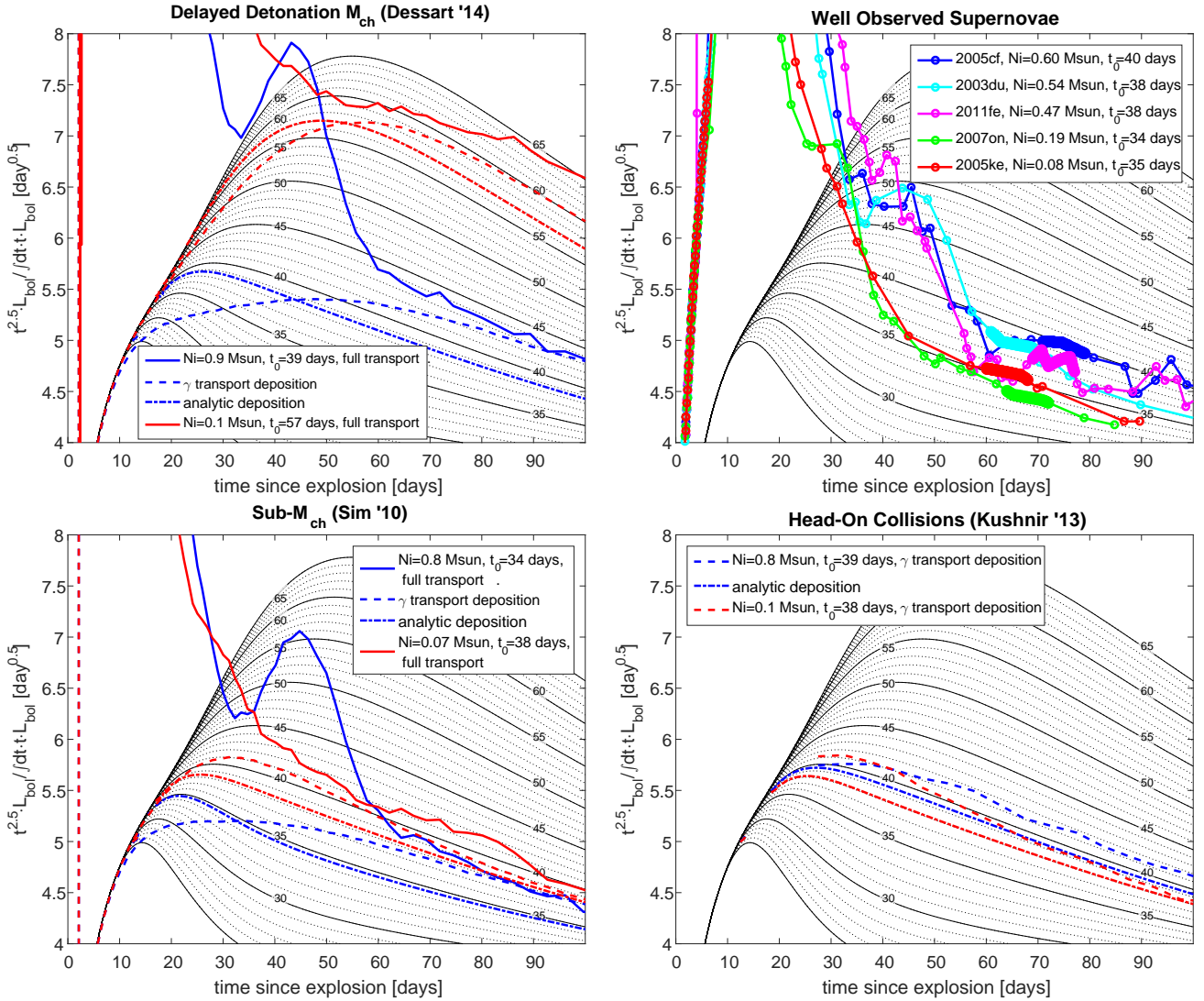


Figure 1. Extracting the gamma-ray escape time t_0 from bolometric light curves. Top right panel: The ratios $L_{\text{bol}}/\int t dt L_{\text{bol}}$ (multiplied by $t^{2.5}$ for convenience) are shown in solid lines for a sample of well observed supernovae: 2005cf (blue, Wang et al. 2009), 2003du (cyan, Stanishev et al. 2007), 2011fe (magenta, Mazzali et al. 2015), 2007on (green, Phillips 2012) and 2005ke (red, Phillips 2012). Analytic ratios of the deposition $Q_{\text{dep}}/\int t dt Q_{\text{dep}}$ are shown for a range of t_0 values using equations (3, 10-12) in black and dotted lines with the values of t_0 labeled on the lines. As can be seen by comparing the observed ratios to the analytic curves at late times $t \gtrsim 60$ days all these supernovae have t_0 in the range of 35 – 40 days. The thicker region on the lines marks the time range in which the value of t_0 used for our analysis was inferred. Top left and two bottom panels: the luminosity ratio functions obtained for synthetic light curves calculated for representative models - M_{ch} delayed detonation models DDC0 (blue) and DDC25 (red) from Dessart et al. (2014), sub- M_{ch} central detonations of WDs with masses $1.15M_{\odot}$ (blue) and $0.88M_{\odot}$ (red Sim et al. 2010) and 2D models of equal mass head on collisions of $0.9M_{\odot}$ WDs (blue) and $0.5M_{\odot}$ WDs (red) from Kushnir et al. (2013). Models with high (blue) and low (red) yields of ^{56}Ni are presented (corresponding to the colors of the bright 2005cf and the faint 2005ke in the top right panel). The ratios $L_{\text{bol}}/\int t dt L_{\text{bol}}$ for the full radiation transfer calculations are shown in solid lines (except for the 2D collision models, for which the radiative transfer simulations have not been performed yet). The ratios $Q_{\text{dep}}/\int t dt Q_{\text{dep}}$ are shown based on γ -ray transport calculations (dashed) and analytically (dash-dotted) using equations (3, 10-12) for all models. The matlab file that created the top right panel, a python file for extracting t_0 and $M_{56\text{Ni}}$ from bolometric light curves, and python and c files for calculating t_0 and Q_{dep} for models are attached to the manuscript as described in appendix §A.

converge beyond ~ 60 days to the analytic expectations that correspond to t_0 values around 35 – 40 days¹. Note that the presented supernovae include both bright and faint events. The uniformity of

t_0 values across the type Ia luminosity range is confirmed for bigger samples (with less quality) in §4. Once t_0 is determined, the ^{56}Ni can be inferred by comparing the amplitude of the light curve to the deposition function calculated with t_0 using Eqs. (10-12). The values of ^{56}Ni extracted in this way are indicated in the legend.

¹ We define t_0 as the average value within the 10-day bin that has the smallest scatter of t_0 values in the range 55-80 days after explosion. The assigned value of the nickel mass is interpolated as the average value over the same time range given this defined t_0 . Varying these arbitrary definitions

over a reasonable range leads to negligible modifications in the assigned t_0 and nickel mass values.

The matlab file that created the top right panel and a python file for extracting t_0 and $M_{56\text{Ni}}$ from bolometric light curves are attached to the manuscript as described in appendix §A.

3 RADIATION TRANSFER SIMULATIONS OF REPRESENTATIVE MODELS

Equations (3) and (10-12) are next compared to results of numerical simulations of both the γ -rays and the UVOIR transport through the ejecta of representative models of Chandrasekhar, sub-Chandrasekhar and the collision scenarios (for the latter, only γ -rays transport was performed, while the full, angle dependent light curves, will be studied in a forthcoming publication).

3.1 Radiation transfer code

Radiation transfer is calculated using URILIGHT, a Monte-Carlo code based on the approximations used in the SEDONA program (Kasen et al. (2006) and references therein). This simulation is based on several physical approximations: 1) homologous expansion. 2) expansion opacities with optical depths using the Sobolev approximation. 3) Local thermodynamic equilibrium (LTE) is assumed for calculating the ionization and excitation states. The atomic line data for the bound-bound transitions, which constitutes the main and most important opacities for these problems, are taken from Kurucz & Bell (1995). A detailed description of this program and comparisons to previously published radiative transfer codes for several benchmark problems are presented in Paper II.

3.2 Representative ejecta models

We present here the deposition function and bolometric light curves of 4 1D ejecta representing extremes of bright and dim SNIa in Chandrasekhar and sub-Chandrasekhar explosion models. The deposition functions for two 2D ejecta that result from extremes of 2D simulations of head-on collisions are also presented. For the Chandrasekhar models, the delayed detonation models DDC0 and DDC25 from Dessart et al. (2014, profiles provided by the authors), corresponding respectively to ^{56}Ni masses of 0.86 and 0.12 M_{\odot} were used. For the sub-Chandrasekhar models, the ejecta profiles generated from simple central explosions of sub Chandrasekhar mass WDs (1.15 and 0.88 M_{\odot}) from Sim et al. (2010, profiles provided by the authors), which have ^{56}Ni masses of 0.81 and 0.07 M_{\odot} , were used. For the collision models, head on collisions of equal mass 0.9 M_{\odot} WDs and of equal mass 0.5 M_{\odot} WDs from Kushnir et al. (2013), which have ^{56}Ni masses of 0.79 and 0.11 M_{\odot} , were used.

In the top left and bottom left panels of figure 1 the calculated synthetic luminosity ratios (solid blue and red) of the 1D Chandrasekhar and sub-Chandrasekhar mass explosions, for which the full radiation transfer was calculated, are shown. Full radiation transfer was not calculated for the 2D collision models in the bottom right panel. The deposition ratios calculated using Monte Carlo gamma-ray transfer are shown for all models (dashed blue and red). As can be seen, beyond about 60 days after explosion (earlier for the faint models) the ratios of the bolometric luminosities converges to that of the deposition, given by Eq. (3), to an accuracy of a few percents (a bump with higher error appears at 130 days in the high luminosity models but we do not consider times > 100 days here where the LTE approximation probably breaks down). Note the bump in the luminosity ratios around 50 days for the brighter events which is due to the IR second maximum and is absent in the lower

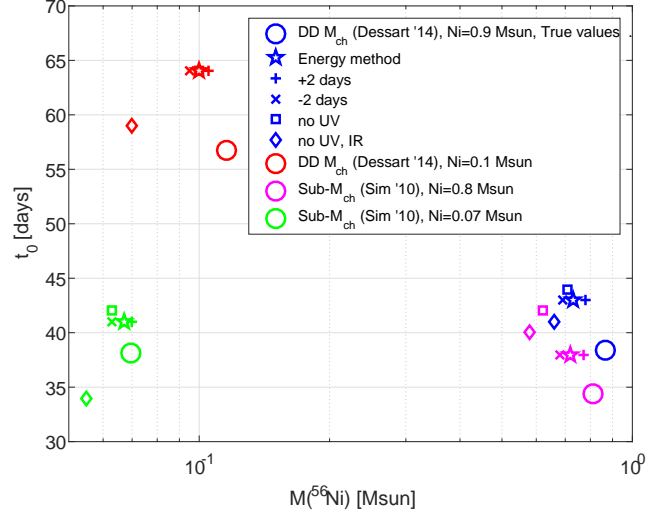


Figure 2. Sensitivity of the ^{56}Ni mass and t_0 to various effects. The t_0 and ^{56}Ni of the 4 ejecta presented in the top-left and bottom-left panels of figure 1: high and low ^{56}Ni mass for M_{Ch} models ejecta from Dessart et al. (2014) (blue and red, respectively) and high and low ^{56}Ni mass for sub- M_{Ch} models ejecta from Sim et al. (2010) (magenta and green, respectively). For each ejecta, the true value of ^{56}Ni mass and t_0 is shown by a large circle, while the value inferred through Eqs. (3) and (10-12), as shown in figure 1, is shown by a star. The values inferred by offsetting the lightcurves by +2(-2) days are marked by +(x) signs, the values inferred by using bolometric lightcurves discarding the UV region ($\lambda < 3000\text{\AA}$) are marked by squares and the values inferred by using bolometric lightcurves discarding the UV and also the IR region ($\lambda > 10000\text{\AA}$) are marked by diamond signs.

luminosity models. The analytic deposition ratios calculated using Eqs. (10-12) are shown for each model in dashed dotted blue and red lines and for a range of t_0 values in black lines. As can be seen, beyond about 60 days after explosion, the analytic estimates agree with the deposition and luminosity ratios to an accuracy better than 10%.

3.3 error budget

We now turn to quantify the accuracy of inferring the ejecta parameters t_0 and ^{56}Ni mass. The effect of various uncertainties on these parameters is shown in figure 2 for the high and low ^{56}Ni mass in Chandrasekhar and sub-Chandrasekhar mass explosions. The actual ^{56}Ni mass and t_0 value (calculated using Eqs. 7 and 8) are shown in the figure as large circles.

basic model accuracy: The values that are obtained by comparing the synthetic light curves to Eqs. (3) and (10-12) in the range $60\text{d} < t < 100\text{d}$ are shown in the figure as large stars. As discussed above, Eqs. (3) and (10-12) are accurate only up to several percent in the considered time range, causing the errors (overestimate) of $\sim 10\%$ t_0 that are obtained. The accuracy in inferring the ^{56}Ni mass given the correct value of t_0 is small ($\sim 3\%$), but the systematic overestimation of t_0 causes a systematic underestimation of ^{56}Ni mass by $\sim 10\%$ as can be seen in the figure.

explosion time: The exact explosion time of observed supernovae is not known precisely. The values of t_0 and ^{56}Ni that are obtained by introducing errors of ± 2 days in the explosion time are shown as pluses and crosses. As can be seen, this has a negligible effect on the luminosity ratio and the deduced t_0 . The ^{56}Ni estimate is affected by $\pm 5\%$ due to such errors in the explosion time.

Partial bolometric lightcurves: The bolometric lightcurves of

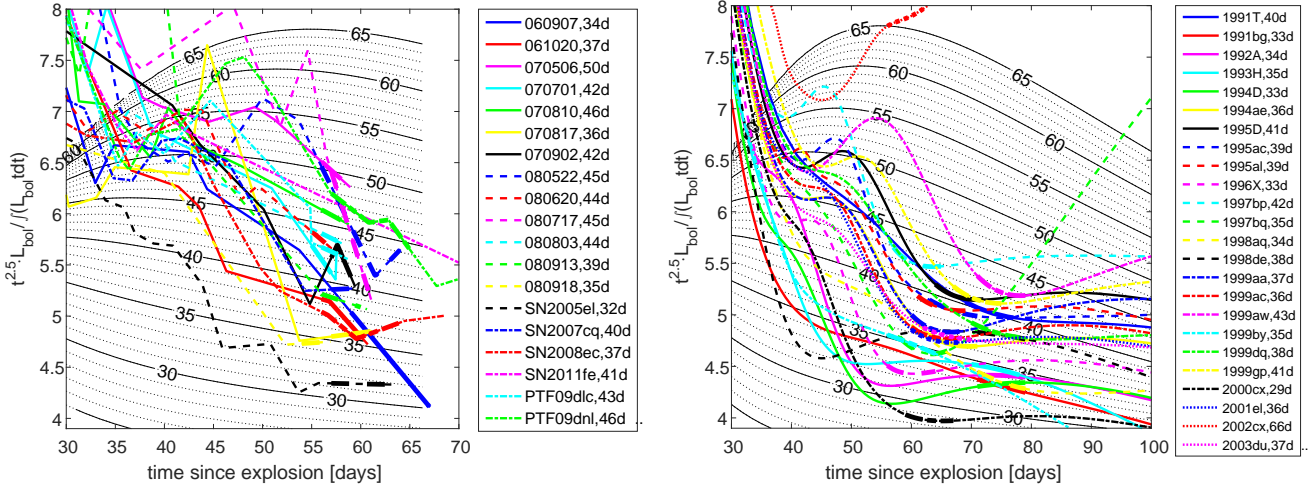


Figure 3. left: Fitting t_0 using bolometric lightcurves for the sample of Scalzo et al. (2014a). The fitting function for each SN is compared to reference (black) lines with different t_0 , as shown in equations (3, 10-12). The legend shows, besides each SN, the fitted value of t_0 , as inferred as the average of t_0 during the time range marked by the thicker region of each line. Note that for the first 13 plotted lightcurves, the first 5 characters were omitted from the legend as they're all identical: 'SNF20'. That is, for example, the full name of the first plotted lightcurve is SNF20060907. The inferred ^{56}Ni masses, in order of their appearance in the legend, are as follows (in units of M_\odot): 0.71, 0.36, 0.67, 0.78, 0.43, 0.36, 0.37, 0.67, 0.34, 0.79, 0.61, 0.48, 0.35, 0.49, 0.54, 0.37, 0.67, 0.54, 0.50. **right:** Fitting for t_0 as in the left panel but for the sample of Stritzinger (2005). The inferred ^{56}Ni masses, in order of their appearance in the legend, are as follows (in units of M_\odot): 0.76, 0.066, 0.22, 0.19, 0.43, 0.68, 0.50, 0.77, 0.44, 0.57, 0.59, 0.53, 0.54, 0.055, 0.51, 0.54, 0.51, 0.07, 0.67, 0.58, 0.32, 0.31, 0.085, 0.29.

SNIa are reconstructed from observations in various regions of the spectrum. For this matter, the visible spectrum is usually taken into account, while UV ($\lambda < \sim 3000\text{\AA}$) and IR ($\lambda > \sim 10000\text{\AA}$) are not always available. While this is justified by the fact that most of the energy is emitted in the optical bands, it introduces some error. The values of t_0 and ^{56}Ni mass that are deduced from the synthetic bolometric light curves when the UV (UV and IR) is not included are shown as squares (diamonds) in the figure and result in errors of up to 10% in t_0 . As can be seen, lack of IR can lead to a significant underestimate of the ^{56}Ni mass by tens of percent.

Rising part of the lightcurve: Finally, In many instances, the rising part of the lightcurve is only partially sampled. The error generated by this deficiency is conservatively estimated in the following way. The rising part of the light curves was replaced with one of two extreme possibilities: either $L = L_{\text{peak}} t^2 / t_{\text{peak}}^2$ (low) or $L = L_{\text{peak}} (1 - (t - t_{\text{peak}})^2 / t_{\text{peak}}^2)$ (high). These cases lead to changes of ± 1 day in the estimate of t_0 , and of $\pm 5\%$ in the deduced ^{56}Ni mass for the 4 models considered.

Hydrodynamic effect of ^{56}Ni decay: When ^{56}Ni decays, it releases an energy per mass equal to about $(2500\text{km/s})^2$. In ejecta with ^{56}Ni concentrated in the middle, the release is comparable to the velocity of the ^{56}Ni and deviation from homologous expansion will occur (e.g. Hoefflich et al. 2017). To check how much this may affect our analysis, we ran a 1D hydrodynamic simulation for an ejecta with extreme ^{56}Ni concentration: exponential velocity density profile with M_{ch} mass and $2E/M = 10^{18}\text{cm}^2/\text{s}^2$ with the ^{56}Ni concentrated in the center. We conservatively assumed that there is no diffusion in the radiation (but ignored the later ^{56}Co decay that occurs when radiation diffuses significantly). The changes in the profiles caused the γ -ray escape time to change from $t_0 = 58$ days (ignoring hydrodynamics) to 54 days. The deviation from homologous expansion introduced an additional error of $\sim 2\%$ in eq.(3). Given these modest corrections in this extreme case, we conclude that the hydrodynamic effect of ^{56}Ni decay can be ignored when inferring the bolometric parameters.

Finally, we note that in addition to the above effects, observed lightcurves might suffer from additional problems such as jitter of measured fluxes and follow-up time shorter than needed. These effects are hard to quantify in general, as they depend on the details of each lightcurve. We further emphasize that even though it was shown in several representing examples that we might systematically overestimate t_0 and underestimate the ^{56}Ni mass, we do not correct for these possible biases in the following sections when fitting for observed light curves since we cannot be sure that this is a general feature for all ejecta.

4 TYPE IA'S HAVE A NARROW RANGE OF GAMMA-RAY ESCAPE TIMES $T_0 \approx 40$ DAYS

In addition to the small sample shown on the right panel of figure 1, we fitted for the sample of 19 SNIa from the Nearby Supernova Factory analyzed in Scalzo et al. (2014a) (which include near-IR corrections, but not UV corrections), as well as for the 24 lightcurves in the sample of Stritzinger (2005) that have low extinction (Galactic+host $E(B - V) < 0.3$), i.e. the same sample as the one used in Kushnir et al. (2013), which, as opposed to the Scalzo sample, contains several lightcurves with low ^{56}Ni mass ($< 0.3M_\odot$). The set of fitting curves for these samples with the reference lines to which they are compared is shown in figure 3, and the inferred value of t_0 for each SN is shown in the legend next to its name. For each SN, the ^{56}Ni mass was inferred from the late time lightcurve using the inferred value of t_0 . Table B1 in appendix B summarizes the determined values of t_0 and ^{56}Ni mass for all the bolometric light curves shown in this work. We note that the uncertainty of the t_0 values inferred from these light curves is larger than the values that were inferred for the light curves shown in the top right panel of figure 1. for the sample of Stritzinger (2005), the inferred values of t_0 seem to reach a minimum and then rise significantly. This is probably due to the template that was used for the late times. But within the time range that was shown above, for well observed light

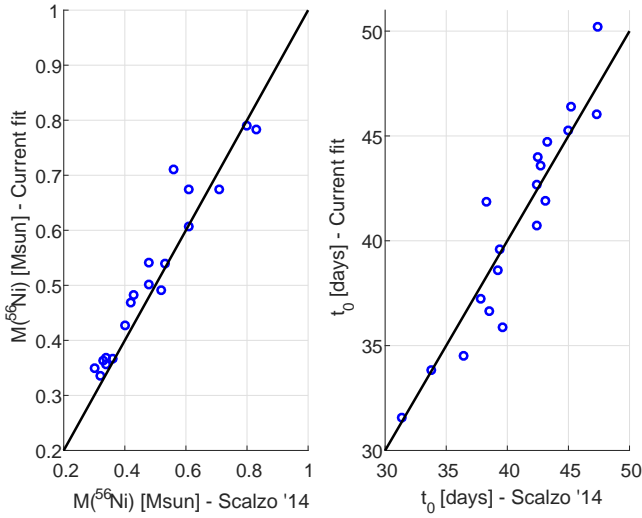


Figure 4. Comparing the inferred values of ^{56}Ni mass (left panel) and of t_0 (right panel) as inferred by Scalzo et al. (2014a) and as obtained in this work.

curves, to be well suited for determining t_0 , i.e. spanning 50-80 days, the uncertainty due to that is mostly limited to ~ 5 days. For the sample of Scalzo et al. (2014a), several of the light curves have data only up to ~ 55 days, which does not allow for much time when t_0 stabilizes on a constant value. In these cases, t_0 was determined from the last 3 days, but we warn the reader that these values are uncertain and might actually have been a bit lower had more data points been available.

A comparison for the values of ^{56}Ni mass and t_0 obtained in this work and their values in Scalzo et al. (2014a), which were inferred using different methods, is shown in figure 4. Despite the different methods, we find similar results for the ejecta parameters: For t_0 , the average value inferred here is 41 days, identical to the average of the inferred values in Scalzo et al. (2014a), and the average absolute difference is 1.3 days. For the ^{56}Ni mass, the average of the sample in Scalzo et al. (2014a) is $0.49M_{\odot}$, while the average value inferred here is $0.52M_{\odot}$ and the average difference between the methods is $0.04M_{\odot}$.

For the sample of Stritzinger (2005), the values we infer for ^{56}Ni mass are systematically 20% – 30% lower than the estimate done by the author using Arnett’s rule. This difference, when compared to the good agreement found for the Scalzo et al. (2014a) sample, is due primarily to the different use of Arnett’s rule by these two authors (the parameter, α was taken as 1 by Stritzinger (2005) and as 1.2 by Scalzo et al. (2014a)), leading to a systematically higher estimate of 20% by Stritzinger (2005). Additionally, Stritzinger (2005) raised his fit for ^{56}Ni mass by 10% to compensate for the lack of UV and IR in the bolometric lightcurve, while we apply no such correction (as such a uniform correction was seen to not be consistent with simulations).

5 OBSERVATIONS ARE CONSISTENT WITH SUB-CHANDRA AND COLLISION MODELS ACROSS THE RANGE OF LUMINOSITIES AND WITH CHANDRASEKHAR MODELS AT THE BRIGHT-END BUT NOT THE FAINT END

As mentioned above, while the physics of SNIa lightcurves include complicated processes, one can constrain progenitor models independently of these processes using solely those ejecta parameters that can be inferred from the bolometric lightcurves. We compare the values found for ^{56}Ni mass and t_0 in the previous section with those values in various progenitor models. The models we looked at were one dimensional delayed detonation models (Dessart et al. 2014), one dimensional sub-Chandrasekhar central detonations of WDs by S. Woosley presented in Moll et al. (2014) (which do not result from explosion models, but serve as benchmarks for the simplest explosion configuration one can imagine, ejecta provided by S. Woosley), similar central detonations of sub-Chandrasekhar WDs from Sim et al. (2010), and two dimensional head on collisions of CO WDs (Kushnir et al. 2013). The comparison of these models with the observed lightcurves presented in the previous section is shown in figure 5. The observations are consistent with the head-on collision model of Kushnir et al. (2013) (as already shown there) and with the sub-Chandrasekhar explosions of Sim et al. (2010) for the whole range of ^{56}Ni masses. They are in possible tension with the sub-Chandrasekhar explosions of Woosley at the high end of the ^{56}Ni masses, though due to the large observational scatter they’re not inconsistent with it, and in addition, the fact that we showed that our fitting method likely overestimates t_0 could resolve some of this tension. The observations are inconsistent with delayed detonations of Chandrasekhar mass WDs as an explosion mechanism for the full range of observed luminosities, since these give values of $t_0 > 50$ days for ^{56}Ni masses below $0.2M_{\odot}$, whereas the observational values of t_0 are all lower than this, even more in the range of such low ^{56}Ni masses (the one observational exception, sn2002cx, is known to be an extremely peculiar, non representative case of SNIa Li et al. (2003)) Moreover, if we take into account the likely overestimation of t_0 in our fitting procedure, the inconsistency becomes even more significant. The observations are consistent with Chandrasekhar mass models at the bright end of the luminosity range.

6 SUMMARY AND DISCUSSION

In this paper we derived and applied a method to derive the gamma-ray escape time t_0 and the ^{56}Ni mass from bolometric light-curves using energy conservation from basic principles. The method is derived in §2, validated using detailed radiation transfer calculations in §3 and applied to observations in §4 (see in particular figures 1 and 5). We find that type Ia’s at all luminosities have t_0 values in a narrow range around 30 – 45 days with weak or no correlation with ^{56}Ni mass.

When applied to the Supernova Factory sample in (Scalzo et al. 2014a) we obtain similar results for $M_{\text{Ni}56}$ and t_0 as those of (Scalzo et al. 2014a, see figure 4). Scalzo et al. (2014a) used a sophisticated code that involved comparison to detailed models and is based on Arnett’s rule. We emphasize that the method presented here is different, simpler and requires less assumptions. Perhaps a more important difference between the two works is that Scalzo et al. (2014a) did not compare the resulting values of t_0 to those of models directly as presented here in figures 1 and 5. Instead they tried

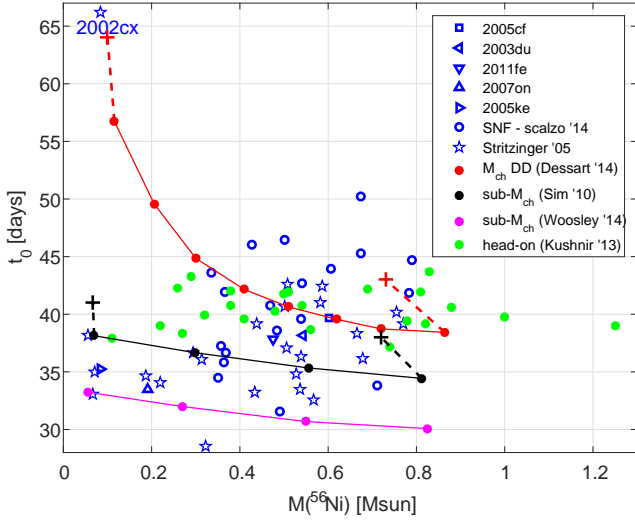


Figure 5. Bolometric Width Luminosity Relation The values of t_0 vs $M(^{56}\text{Ni})$ ('width' as function of 'luminosity') for a sample of SNe (blue marks, as detailed in the legend), and for different progenitor models: delayed detonation (red, Dessart et al. (2014)), two different sets of calculations of sub-Chandrasekhar central explosions (black - Sim et al. (2010), and magenta - S. Woosley presented in Moll et al. (2014)) and head-on collisions (green - Kushnir et al. (2013)). For 4 of the models, a dotted line is shown connecting the true ejecta values (marked by filled circles) to the values inferred by the fitting process (+ signs), indicating that a systematic small offset might be present between observed and true values.

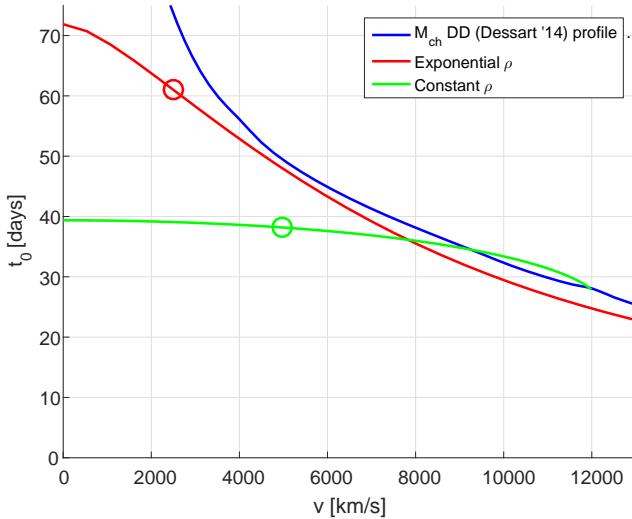


Figure 6. t_0 as a function of the location of the ^{56}Ni within the ejecta for various density profiles (assuming it is concentrated in a thin shell): the lowest ^{56}Ni mass delayed detonation from Dessart et al. (2014) (blue line), exponential and constant profiles (red and green). The circles mark the velocity at the edge of the inner $0.1 M_{\odot}$.

to deduce the ejecta mass from the values of t_0 and ^{56}Ni by using explosion simulations for calibration and compared the deduced masses to those of various models. This last step depends on the calibration model and may lead to misleading results. In fact, different models with different ejecta masses can have very similar t_0 and ^{56}Ni . For example, the collision models and the sub- M_{ch} have similar values of t_0 but significantly different ejecta masses at the high ^{56}Ni end. In particular the collision of two $0.9 M_{\odot}$ WDs (total mass

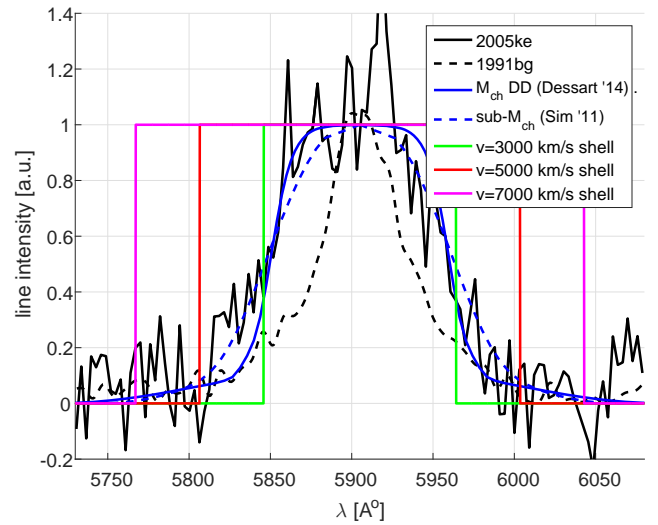


Figure 7. Emission line of ^{56}Co at $\sim 5900\text{\AA}$ observed in two low ^{56}Ni mass SN: sn1991bg (Turatto et al. 1996) and sn2005ke (Folatelli et al. 2013) (dashed and solid black lines), along with line-of-sight ^{56}Ni mass distribution, serving as indicators for line shapes, for low ^{56}Ni mass ejecta for delayed detonations (Dessart et al. 2014) and central sub-Chandrasekhar WD explosions (Sim et al. 2010) (solid and dashed blue lines), as well as line shapes for thin shells of ^{56}Co at velocities of 3000, 5000 and 7000 km/s (green, red and magenta solid lines, respectively).

of $1.8 M_{\odot}$, $t_0 = 39\text{d}$, $^{56}\text{Ni} = 0.79 M_{\odot}$) and the central detonation of a WD with mass of $M = 1.15 M_{\odot}$ ($t_0 = 35\text{d}$, $^{56}\text{Ni} = 0.81 M_{\odot}$) have very similar t_0 and ^{56}Ni while having masses that differ by more than 50%. **The total mass cannot be extracted from t_0 and the ^{56}Ni mass. However, it can easily be directly compared to the values of any multi-D explosion model.** Finally we note that the sample in Scalzo et al. (2014a) does not include low luminosity type Ia's. As can be seen in figure 5, the different models deviate most significantly at the faint end and thus low luminosity type Ia's, although constituting only a small fraction of the total observed SNIa, play a significant role in differentiating between different explosion mechanisms. that may explain the full range of luminosities. We note that it is also possible that different mechanisms produce type Ia supernovae with different luminosities, and Chandrasekhar mass models are not disfavored based on their bolometric properties as progenitors for bright type Ia's.

The ^{56}Ni and t_0 deduced from the observations are compared to models in figures 1 and 5. We find that low luminosity supernovae are inconsistent with delayed-detonation Chandrasekhar mass models in agreement with the findings of several recent works (Kushnir et al. 2013; Scalzo et al. 2014a,b; Blondin et al. 2017; Dhawan et al. 2017).

The large escape times for low ^{56}Ni masses in M_{ch} models, are due to the large mass present at velocities beyond the ^{56}Ni . Given the uncertainty of the Chandrasekhar mass explosion models, it is instructive to ask if the problem can be alleviated by changing the distribution of the ^{56}Ni in the ejecta. As can be seen in figure 6, the ^{56}Ni has to be moved out to velocities of ~ 7000 km/s in order to reduce the escape time to observed values of $t_0 \sim 40$ days. Such high ^{56}Ni velocities are inconsistent with nebular spectra of low luminosity type Ia supernovae (e.g. Mazzali et al. 1998, and figure 7) which imply velocities $v \lesssim 5000$ km/s. We note that in an extreme case of a Chandrasekhar-mass ejecta with a homogeneous density distribution, both the line-width and the bolometric properties may

be accounted for. Such ejecta are not expected in thermonuclear explosions as far as we know. Recently [Hoefflich et al. \(2017\)](#) showed results of a series of radiation transfer calculations that are claimed to agree with type Ia observations across the type Ia brightness range. Based on the results here, either the bolometric luminosity or the nebular line widths of these models (both are not shown in the paper) are likely inconsistent with observations of low-luminosity type Ia's.

Direct collisions and sub-Chandrasekhar models have a narrow range of t_0 in agreement with observations. The existence of such examples, and in particular the collisions where the ignition of a detonation is robust and resolved in global simulations, supports the existence of a single mechanism for type Ia supernovae that explains the entire range of brightness.

ACKNOWLEDGMENTS

We thank Doron Kushnir, Subo Dong, Chris Burns, Mark Phillips, Stuart Sim, Stephane Blondin, Stan Woosley, Bob Kurucz, and Peter Hoefflich for useful discussions and clarifications. We thank Charling Tao and Richard Scalzo for help with the bolometric light curves of the Supernova Factory. We thank Stuart Sim, Stephane Blondin, Stan Woosley and Daniel Kasen for providing ejecta and radiation transfer results. This research was supported by the ICORE Program (1829/12) and the Beracha Foundation.

APPENDIX A: ATTACHED CODE AND DATA FILES

There are two .zip files attached to this paper in the online supplementary material which can also be accessed using the following dropbox links:

AnalyzeLightCurves.zip at

<https://www.dropbox.com/s/ngsnhwof3ron5og/>

AnalyzeLightCurves.zip?dl=0

AnalyzeModels.zip at

<https://www.dropbox.com/s/5mculjy7p5n0kyw/>

AnalyzeModels.zip?dl=0

Each of these compressed files contains a folder with additional files and folders as described below.

A1 Light Curve Analysis Files

The file AnalyzeLightCurves.zip, contains a folder with matlab and python Jupyter notebooks that allow the analysis of bolometric light curves along with data files of the supernovae presented in figure 1 as important examples. The following files are included in the folder:

- (i) Bolometric UVOIR light curves of the 5 well observed SNe presented in the top right panel of figure 1. The references are described in the caption and the explosion time estimates are explained in the header of the files. The five files are: sn2003du_Stanishev07.txt, sn2005cf_Wang09.txt, sn2005ke_Phillips12.txt, sn2007on_Phillips12.txt, sn2011fe_Mazzali15.txt. Each file contains two columns-time in days and Log10 of the luminosity in ergs per second.
- (ii) SNiA_t0_from_bolometric.m : A matlab file that creates the top right panel of figure 1 and can be used to extract the value of t_0 for a given bolometric light curve. It uses the attached light curve files and thus needs to be run from the folder in which they are stored.

- (iii) SNiA_t0_MNi_from_bolometric.ipynb : A python Jupyter notebook that allows the extraction of t_0 and the ^{56}Ni mass from bolometric light curves by manual fitting based on equations (3, 10-12). This file also uses the (same) bolometric data files and needs to be run from the folder where they are stored.

A2 Model Analysis Files

The file AnalyzeModels.zip contains a folder with files for analyzing model ejecta and performing Monte Carlo gamma-ray transfer calculations. It contains the following files and folders.

- (i) There are three folders with ejecta files containing the total density and the ^{56}Ni distribution for the models described in §3.2
 - ** DDC_Blondin13/ : M_{ch} 1D delayed detonation models from [Dessart et al. \(2014\)](#)
 - ** SubChandraWoosley14/ : 1D sub- M_{ch} central detonations of WDs with different masses by S. Woosley and presented in [\(Moll et al. 2014\)](#)
 - ** Col2DKushnir13/: 2D direct collision models from [Kushnir et al. \(2013\)](#). Since these 2D ejecta files take up some memory, only equal mass collisions are provided. All ejecta from [Kushnir et al. \(2013\)](#) in a similar format can be accessed in the following dropbox link: https://www.dropbox.com/sh/7g25m6zcv4nva2u/AABQwpExS_5JZNE68-lsRBbTa?dl=0
 The files of these models are read by the python Jupyter notebook described next.
- (ii) SNiA_Analyze_Models.ipynb : A python Jupyter notebook that allows the extraction of t_0 and the calculation of gamma-ray transfer for model ejecta. In particular this file reads and allows the analysis of the ejecta in the model folders above and needs to be run from a folder that contains the model folders. The file allows gamma-ray transfer calculations using a c-based code which is attached in the folder MonteCarloCode. In order for the Jupyter notebook to access the Monte Carlo code, the MonteCarloCode folder needs to be stored at the same folder as the notebook.
- (iii) MonteCarloCode : A folder that contains a gamma-ray transfer Monte Carlo code written in c. It can be run directly but is easiest to use with the Jupyter notebook. The main outputs are log_output.txt which contain t_0 and output.txt that contains the total deposition by gamma-rays and positrons as a function of time. The provided examples are 1D and 2D, but the code contains functions for calculating the 3D ejecta.

APPENDIX B: T_0 AND ^{56}Ni MASS FROM LIGHT CURVES

Table B1 summarizes the sample of bolometric light curves analyzed in this work, along with the inferred values of t_0 and ^{56}Ni mass. Note that SN2011fe appears both in [Mazzali et al. \(2015\)](#) and in the sample of [Scalzo et al. \(2014a\)](#), yielding similar results, and SN2003du appears both in [Stanishev et al. \(2007\)](#) and in [Stritzinger \(2005\)](#), yielding similar results for t_0 but different results for the ^{56}Ni mass, due to vastly different distances to the source used in these two.

REFERENCES

- Ambwani K., Sutherland P., 1988, *ApJ*, **325**, 820
 Arnett W. D., 1969, *Ap&SS*, **5**, 180
 Axelrod T. S., 1980, PhD thesis, California Univ., Santa Cruz.

Table B1. observed SN sample.

name	t_0 [days]	^{56}Ni [M_{\odot}]	ref for Bolometric
2005cf	40	0.60	Wang et al. (2009)
2003du	38	0.54	Stanishev et al. (2007)
2011fe	38	0.47	Mazzali et al. (2015)
2007on	34	0.19	Phillips (2012)
2005ke	35	0.085	Phillips (2012)
1991T	40	0.76	Stritzinger (2005)
1991bg	33	0.066	Stritzinger (2005)
1992A	34	0.22	Stritzinger (2005)
1993H	35	0.19	Stritzinger (2005)
1994D	33	0.43	Stritzinger (2005)
1994ae	36	0.68	Stritzinger (2005)
1995D	41	0.50	Stritzinger (2005)
1995ac	39	0.77	Stritzinger (2005)
1995al	39	0.44	Stritzinger (2005)
1996X	33	0.57	Stritzinger (2005)
1997bp	42	0.59	Stritzinger (2005)
1997bq	35	0.53	Stritzinger (2005)
1998aq	34	0.54	Stritzinger (2005)
1998de	38	0.055	Stritzinger (2005)
1999aa	37	0.51	Stritzinger (2005)
1999ac	36	0.54	Stritzinger (2005)
1999aw	43	0.51	Stritzinger (2005)
1999by	35	0.070	Stritzinger (2005)
1999dq	38	0.67	Stritzinger (2005)
1999gp	41	0.58	Stritzinger (2005)
2000cx	29	0.32	Stritzinger (2005)
2001el	36	0.31	Stritzinger (2005)
2002cx	66	0.085	Stritzinger (2005)
2003du	37	0.29	Stritzinger (2005)
SNF20060907-000	34	0.71	Scalzo et al. (2014a)
SNF20061020-000	37	0.36	Scalzo et al. (2014a)
SNF20070506-006	50	0.67	Scalzo et al. (2014a)
SNF20070701-005	42	0.78	Scalzo et al. (2014a)
SNF20070810-004	46	0.43	Scalzo et al. (2014a)
SNF20070817-003	36	0.36	Scalzo et al. (2014a)
SNF20070902-018	42	0.37	Scalzo et al. (2014a)
SNF20080522-011	45	0.67	Scalzo et al. (2014a)
SNF20080620-000	44	0.34	Scalzo et al. (2014a)
SNF20080717-000	45	0.79	Scalzo et al. (2014a)
SNF20080803-000	44	0.61	Scalzo et al. (2014a)
SNF20080913-031	39	0.48	Scalzo et al. (2014a)
SNF20080918-004	35	0.35	Scalzo et al. (2014a)
SN2005el	32	0.49	Scalzo et al. (2014a)
SN2007cq	40	0.54	Scalzo et al. (2014a)
SN2008ec	37	0.37	Scalzo et al. (2014a)
SN2011fe	41	0.47	Scalzo et al. (2014a)
PTF09dlc	43	0.54	Scalzo et al. (2014a)
PTF09dnl	46	0.50	Scalzo et al. (2014a)

Blondin S., Dessart L., Hillier D. J., Khokhlov A. M., 2017, *MNRAS*, **470**, 157

Branch D., Chau Dang L., Baron E., 2009, *PASP*, **121**, 238

Burns C. R., et al., 2014, *ApJ*, **789**, 32

Dessart L., Blondin S., Hillier D. J., Khokhlov A., 2014, *MNRAS*, **441**, 532

Dhawan S., Leibundgut B., Spyromilio J., Blondin S., 2017, *A&A*, **602**, A118

Dong S., Katz B., Kushnir D., Prieto J. L., 2015, *MNRAS*, **454**, L61

Folatelli G., et al., 2013, *ApJ*, **773**, 53

Hillebrandt W., Niemeyer J. C., 2000, *ARA&A*, **38**, 191

Hoeflich P., Khokhlov A., Wheeler J. C., Phillips M. M., Suntzeff N. B., Hamuy M., 1996, *ApJ*, **472**, L81

Hoeflich P., et al., 2017, *ApJ*, **846**, 58

Hoyle F., Fowler W. A., 1960, *ApJ*, **132**, 565

Jeffery D. J., 1999, ArXiv Astrophysics e-prints,

Junde H., 1999, *Nuclear Data Sheets*, **86**, 315

Kasen D., Woosley S. E., 2007, *ApJ*, **656**, 661

Kasen D., Thomas R. C., Nugent P., 2006, *ApJ*, **651**, 366

Katz B., Dong S., 2012, preprint, ([arXiv:1211.4584](https://arxiv.org/abs/1211.4584))

Katz B., Kushnir D., Dong S., 2013, preprint, ([arXiv:1301.6766](https://arxiv.org/abs/1301.6766))

Kerzendorf W. E., Taubenberger S., Seitenzahl I. R., Ruiter A. J., 2014, *ApJ*, **796**, L26

Khokhlov A. M., 1991, *A&A*, **245**, 114

Kurucz R. L., Bell B., 1995, Atomic line list

Kushnir D., Katz B., Dong S., Livne E., Fernández R., 2013, *ApJ*, **778**, L37

Li W., et al., 2003, *PASP*, **115**, 453

Livne E., 1990, *ApJ*, **354**, L53

Maoz D., Mannucci F., Nelemans G., 2014, *ARA&A*, **52**, 107

Mazzali P. A., Cappellaro E., Danziger I. J., Turatto M., Benetti S., 1998, *ApJ*, **499**, L49

Mazzali P. A., Nomoto K., Cappellaro E., Nakamura T., Umeda H., Iwamoto K., 2001, *ApJ*, **547**, 988

Mazzali P. A., et al., 2015, *MNRAS*, **450**, 2631

Moll R., Raskin C., Kasen D., Woosley S. E., 2014, *ApJ*, **785**, 105

Nugent P., Phillips M., Baron E., Branch D., Hauschildt P., 1995, *ApJ*, **455**, L147

Pakmor R., Kromer M., Röpke F. K., Sim S. A., Ruiter A. J., Hillebrandt W., 2010, *Nature*, **463**, 61

Phillips M. M., 1993, *ApJ*, **413**, L105

Phillips M. M., 2005, in Turatto M., Benetti S., Zampieri L., Shea W., eds, *Astronomical Society of the Pacific Conference Series Vol. 342, 1604-2004: Supernovae as Cosmological Lighthouses*. p. 211

Phillips M. M., 2012, *Publ. Astron. Soc. Australia*, **29**, 434

Pinto P. A., Eastman R. G., 2000, *ApJ*, **530**, 744

Pinto P. A., Eastman R. G., 2001, *New Astron.*, **6**, 307

Pskovskii I. P., 1977, *Soviet Ast.*, **21**, 675

Rosswog S., Kasen D., Guillochon J., Ramirez-Ruiz E., 2009, *ApJ*, **705**, L128

Scalzo R., et al., 2014a, *MNRAS*, **440**, 1498

Scalzo R. A., Ruiter A. J., Sim S. A., 2014b, *MNRAS*, **445**, 2535

Shen K. J., Bildsten L., 2014, *ApJ*, **785**, 61

Shen K. J., Kasen D., Miles B. J., Townsley D. M., 2017, preprint, ([arXiv:1706.01898](https://arxiv.org/abs/1706.01898))

Sim S. A., Röpke F. K., Hillebrandt W., Kromer M., Pakmor R., Fink M., Ruiter A. J., Seitenzahl I. R., 2010, *ApJ*, **714**, L52

Stanishev V., et al., 2007, *A&A*, **469**, 645

Stritzinger M., 2005, PhD thesis, Technical Univ. Munich

Swartz D. A., Sutherland P. G., Harkness R. P., 1995, *ApJ*, **446**, 766

Turatto M., Benetti S., Cappellaro E., Danziger I. J., Della Valle M., Gouiffes C., Mazzali P. A., Patat F., 1996, *MNRAS*, **283**, 1

Wang X., et al., 2009, *ApJ*, **697**, 380

Woosley S. E., Taam R. E., Weaver T. A., 1986, *ApJ*, **301**, 601

Wygoda N., Katz B., Elbaz Y., 2018, preprint, ([arXiv:1805.06907](https://arxiv.org/abs/1805.06907))

This paper has been typeset from a $\text{\TeX}/\text{\LaTeX}$ file prepared by the author.